Journal of Power Sources 657 (2025) 238231

Contents lists available at ScienceDirect

Journal of Power Sources

journal homepage: www.elsevier.com/locate/jpowsour

Adapting serpentine flow fields for application in large-scale vanadium redox flow battery cells through marginal design modifications

Raveendra Gundlapalli *, Gaurav Jaiswal

Department of Chemical Engineering, Indian Institute of Technology (BHU) Varanasi, Uttar Pradesh, India, 221005

HIGHLIGHTS

- Simulations on electrolyte distribution is performed over cell sizes 100–2025 cm^2.
- Uniform flow characteristic of serpentine flow field is retained with cell size.
- Substrate flow and residence time of electrolyte increased with cell size.
- Proposed marginal modifications support the use of serpentine for large size cells.
- Alternate channel dimensions and partial slice in electrode are studied.

GRAPHICAL ABSTRACT

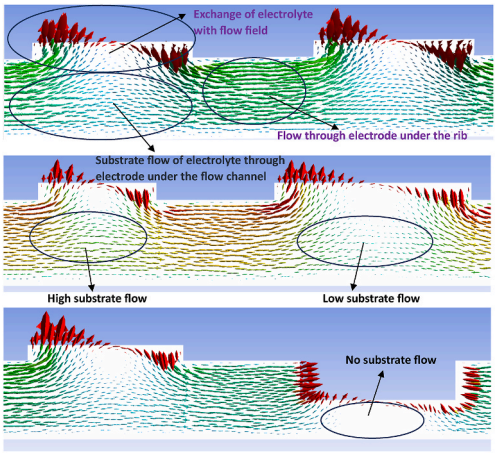

ARTICLE INFO

Keywords:
Redox flow batteries
Scale-up
Serpentine flow field
Channel dimensions
Electrolyte distribution
Energy density

ABSTRACT

Vanadium redox flow batteries are promising devices for large-scale and long duration energy storage. The independent rating of power and energy of these batteries enable customized scalability. Nevertheless; the low energy density of these systems hampering their penetration into energy market. Flow field on bipolar plate enable efficient transportation of electrolyte through electrode and increases degree of utilization of electrolyte leading to enhanced extraction of its intrinsic energy. Serpentine flow field is well-known for uniform flow distribution, however on lab-scale cells of size up to 100 cm^2. In view of stack-scale requirement, the features of serpentine are explored in the cell size window of 100–2025 cm^2. Studies revealed that the uniform distribution feature is retained over the cell size, however with increase in substrate flow and residence time of electrolyte species leading to reduced electrochemical performance. The proposed marginal design modifications, in the form of alternate wide and narrow channels and segmenting traverse distance of electrolyte in electrode, produced 17 % and 3 % higher energy density and energy efficiency, respectively compared to conventional serpentine. These marginal design modifications enable the translation of beneficial features of serpentine flow field in the scale-up of redox flow batteries.

* Corresponding author.
E-mail address: raveendra.che@iitbhu.ac.in (R. Gundlapalli).

https://doi.org/10.1016/j.jpowsour.2025.238231
Received 12 June 2025; Received in revised form 4 August 2025; Accepted 23 August 2025
Available online 26 August 2025

1. Introduction

The modern energy sector is diversifying its verticals and energy storage is occupying major share in it. An energy storage system requires long life, high efficiency, scalability, safety and low cost [1]. Electrochemical energy storage systems are more supportive to guarantee the resilience and stability of the electrical supply, especially at large-scale and long-duration [2]. Redox flow batteries (RFB) are more prominent for large-scale and long duration storage needs. These batteries are distinguished from conventional solid-state batteries like Li-ion and Lead-acid in terms of power to energy ratings. Power is translated from number of cells in a battery stack and energy is rated from the amount of electrolyte that stored outside the stack. This independency in the design of power to energy ratio enabling inherent modularity and flexibility for energy storage users to scale the system for diverse applications like data centres, dwellings, charging stations and several grid-scale applications including backup power, voltage support, peak shaving and frequency modulation [3–7]. The RFB market share is expected to reach billions of dollars by 2031 [8]. Among several RFBs; vanadium redox flow battery (VRFB) is the most researched and successful technology and has reached effective commercial fruition. This has been accomplished by VRFB due to usage of same metal ion in both positive and negative electrolytes avoiding cross-contamination of electrodes and due to long-life of electrolyte attributed to negligible self-discharge [9–11].

In spite of successful deployment; the VRFB systems are facing difficulty to penetrate into modern energy market due to high capital costs, which are closely associated with low power density and suboptimal electrolyte utilization. Several studies on VRFB cells have been reported with considerable improvements in performance characteristics, with most of them explored at cell size of up to 100 cm^2 and very few beyond this size. On the stack-scale applications which are required to meet the real-time dynamics; cell size should be as large as possible typically in the window of 600–1500 cm^2 and beyond subject to material properties and system adaptability [12–15]. Performance metrics of the VRFB have been improved through material treatments [16–18], controlling operating conditions [19–21], and design of stack layout [7,22]. These methods involve significant additional material cost and vigorous system management. There is another approach of improving performance characteristics without involving additional cost and management, which is by engraving a flow field on bipolar plate. In order to achieve high power density and extract maximum possible amount of intrinsic energy of electrolyte in a charge-discharge life cycle, the active area of electrode should be fully and equally supplied with electrolyte reactant species and the products of electrochemical reaction should be removed without accumulation. This distribution mechanism can be tailored by employing a flow field on bipolar plate [23].

Xu et al., [24] explored the performance metrics of VRFB with serpentine flow fields (SFF) on a cell area of 16 cm^2 and found that the efficiency was increased by 5 % with flow fields compared to the case without flow fields. Maurya et al., [25] compared the performance with and without flow field by employing serpentine and interdigitated configurations on a cell area of 25 cm^2. It was posted that the flow fields have given low pumping losses (pressure drop) and improved electrochemical performance, and recommended serpentine for better flow uniformity towards high current density operations. Messaggi et al., [26] performed experimental and computational investigations on a cell area of 25 cm^2 with serpentine and interdigitated flow fields and demonstrated superior electrochemical performance for serpentine and reduced pressure drop for interdigitated. Similar results were reported by Kumar and Jayanti [27] on a cell area of 100 cm^2, that the overpotentials are reduced with flow fields attributing to improved electrolyte distribution and resulted 30 % higher power density compared to cells without flow field, with recommendation of serpentine for uniform distribution of electrolyte over interdigitated. Macdonald and Darling [28] were performed simulation studies on cell area of 100 cm^2 with serpentine and interdigitated, and through velocity contours in the electrode and flow channels; the study reported lower non-uniformity of electrolyte over the electrode for serpentine compared to interdigitated; however, at the expense of higher pressure drop. Similarly, several other studies demonstrated uniform distribution of electrolyte with high pressure drop as feature of serpentine and uneven electrolyte distribution with low pressure drop as feature of interdigitated flow fields [29–32].

There have been only few studies reported on the impact of flow fields and their design towards stack-scale applications which typically demand the cell size in the window of 600–1500 cm^2. Knudsen et al., [33] through their numerical study on the analysis of flow behaviour in high-power flow batteries up to a cell size of 400 cm^2, recommended flow structure visualization as an important tool to determine the quality of electrolyte distribution. Although their study demonstrated non-linear scale-up of pressure drop with cell size, they appealed extended studies on large size cells in the range of 1000 cm^2 for further optimization in the cell design. Sun et al. investigated various pathways like; geometric similarity, channel length extension, maintaining same pressure drop and splitting the flow field; to scale-up the flow fields to a cell size of 900 cm^2. In this process, it was recognized that the splitting phenomenon outperformed the other scaling methods, however at the cost of increased pressure drop. In the other pathways, the increased number of channels attributed to channel length extension, wider channels attributed to geometric similarity resulted in reduced uniformity of electrolyte distribution at large cell size of 900 cm^2 [34]. Similar investigation; through numerical simulations using serpentine flow field on a cell size of 1225 cm^2, was reported by Su et al. by involving channel length extension, geometric similarity, multi-parallel channels, splitting into subzones and combination of splitting and parallel channels. Although the authors claimed that the “shortening of supply path” and “enhancing the supply rate” would be the key factors in determining uniform distribution of electrolyte, their results show that multi-parallel structure outperform others. As the pathways of “splitting into subzones” and the combination of “split-area & parallel channel” lead to shortening the electrolyte path from inlet to outlet, these configurations could have been given better performance than the claimed multi-parallel structure. This hypothetical conflict might be due to the validation of model with experimental results on cell size of 9 cm^2 and then evaluating the metrics of performance through model on the cell size of 1225 cm^2 [35] where the dynamics of distribution changes significantly and differently compared to that of on 9 cm^2. The flow distribution and the required electrolyte supply rate for a serpentine flow field is proved to be dependent on cell area and the fraction of electrolyte that penetrate to electrode from flow field [36]. At equal area-specific supply rate, the local momentum increases with cell size and therefore the penetration of electrolyte through electrode increases leading to requirement of lower area-specific flow rates on larger cells compared to smaller cells. This dynamic dependence of cell performance on supply rate and corresponding electrolyte penetration fraction through porous electrode should be considered in the model to predict performance with serpentine flow field in the scale-up from lab-scale to stack-scale. Our earlier studies on large cell size up to 1500 cm^2 [37] also recommended splitting of the flow field as better pathway to attain considerable uniformity of electrolyte distribution with reduced pumping losses to achieve standard electrochemical performance of the cells.

Any flow field design should enable unform electrolyte distribution through the electrode with possible quick evacuation of reaction products from it, shorter electrolyte flow paths through electrode, low pressure drop, low ohmic contact resistance between bipolar plates and electrode, high mass transfer coefficient and low fabrication cost. Important configurations which enable these features are dimension of flow channels (length, width and depth) and dimension of electrode (thickness and compression ratio). The coupled transport process between flow field and electrode is an important element to investigate in achieving high power density through high operating and limiting

current densities. In view of low permeability of electrode, velocity of electrolyte is much smaller in it than in the flow channels and therefore; volumetric penetration of electrolyte through electrode will be less in general. This reflects the availability of reactants in due course of reaction along the flow path of electrolyte through electrode and consequently affects the cell performance if the products of reaction are not evacuated with simultaneous replenishment of active sites with fresh reactants. In addition to this, electrolyte penetrates more near the inlet zone compared to outlet zone attributed to higher momentum near the entrance [14,38–43]. In order to extract larger amount of intrinsic energy of electrolyte at low parasitic losses, electrolyte distribution within the porous electrode should be well designed by understanding the convective transport of electrolyte through the electrode and exchange of products and reactants between the flow field and electrode associated with concentration driven diffusive transport and pressure driven convective transport.

Specific flow field designs like detached serpentine, rotary serpentine, split-merged serpentine, blocks and obstructions in flow field, enhanced-split in flow field, wide and narrow channels in flow field, and bio-inspired patterns have been investigated to understand and improve the transport of electrolyte in the porous electrode [44–52]. Sun et al., [44] proposed detachment of serpentine flow field between bipolar plate and porous electrode in such a way that inflow of electrolyte through bipolar plate while the outflow; only through porous electrode on a cell area of 9 cm^2. In view of the forced convective transport from flow channels to porous electrode, the operating current density and energy efficiency both were increased compared to conventional serpentine. For a current density of 100 mA cm^{-2} at flow rate of 2 ml min^{-1}. cm^{-2}, the detached configuration achieved 66.5 % energy efficiency. The results also claimed better performance at low electrode compression (at 20 %) and at high electrolyte flow rate (at 2 ml min^{-1}. cm^{-2}). In view of recommended electrode compression ratio of 35–50 % [39,53] and electrolyte flow rate of 0.6–1.5 ml min^{-1}. cm^{-2} for improved electrochemical performance with reduced parasitic losses [10,21], energy efficiency in the window of 70–75 % [12,21,36,54] at the operated current density for stack-scale operations, this design may not be recommended for scale-up, unless fine-tuned for larger cell size. Lu et al., [45] introduced rotary design in the serpentine configuration which has continuous flow path similar to conventional serpentine but moves back and forward between the inlet and outlet. This study on a cell area of 100 cm^2 through a 3-D multi-physical model (which is validated using conventional serpentine) predicted better electrochemical performance and improved distribution of species over the electrode area for rotary design compared to conventional serpentine. However, the flow rates used for prediction are in the window of 1.2–9 ml min^{-1}. cm^{-2} which are futile for stack-scale applications. The design needs to be explored experimentally for real-time performance and at the standard required flow rates. Sharma and Kumar [46] investigated split-merge combination of serpentine on a cell area of 10 cm^2 by employing the flow rates from 3 to 18 ml min^{-1}. cm^{-2}. Although the results claim to have low charge-transfer resistance for the designed configuration compared to conventional serpentine, the study needs to be explored at larger cell size and at practically possible stack-scale flow rates. Partial blocks; restricting the channel depth, were introduced near the U-turn of the serpentine flow path on a cell area of 100 cm^2 and the corresponding simulation studies resulted 3.7 % higher energy efficiency compared to conventional serpentine [47]. Another numerical study on cell area of 13 cm^2 investigated in-plane gradient in the channel width becoming wider to narrow or vice versa from inlet to outlet. The gradience in the channel width enhanced the pressure difference and resulted in improved convective transport of species from flow channels to porous electrode and in view of this, the configuration predicted 3 % higher operating current density compared to conventional serpentine [49]. Recently, bionic and nature-mimicking flow fields are investigated, through numerical simulations, on the cell areas of 4 cm^2 and 9 cm^2 to achieve more uniform distribution in the porous electrode. The local branching and diversions of the channel flow improved local uniformity and predicted improved performance compared to conventional flow fields [51,52]. However, the similar uniformity index should be explored at relevant cell size to use the nature inspired flow fields in redox flow batteries.

In view of increased pressure drop and decreased flow uniformity with cell size irrespective of configuration of flow field, the coupled distribution of electrolyte across the flow field and porous electrode should be well investigated to achieve flow uniformity with possible reduction in pressure drop. Although the split design in the flow field is recommended for stack-scale applications to reduce pressure drop, it suffers in achieving local uniform convective transport and exchange of species between flow field and electrode. Other design variants [44–52] which could able to improve uniformity of transport of electrolyte through porous electrode; are explored at small cell sizes (below 100 cm^2) and at very high flow rates. The scale-up of respective designs need further investigation and should be configured to operate at practically suitable electrolyte supply rates. In view of much-needed flow field configurations for stack-scale, the present study introduces marginal design changes in conventional serpentine towards larger cell size.

In view of impact of local geometrical modifications of flow field on the cell performance, this study involves the incorporation of marginal design changes to the serpentine flow field (SFF) and assessing their influence on hydrodynamic and electrochemical performance. The proposed design changes are the incorporation of wide and narrow channel combination and creating partial slicing in the porous electrode. Conventional SFF has been experimentally characterized on cells of area 100 cm^2 and 625 cm^2 by measuring pressure drop, charge-discharge life cycles and power density curves. In order to experience the effect of increase in cell area on electrolyte distribution using SFF, computational fluid dynamic (CFD) simulations have been performed. Calibration of simulations is carried out with the experimentally measured pressure drop on cells of 100 cm^2 and 625 cm^2 and further simulations have been produced to a cell size of 2025 cm^2 in order to investigate the pressure drop and electrolyte distribution pattern. The proposed design modifications have been explored on cell size 625 cm^2 through both computational and experimental routes and discussed in detail. These proposed designs retain the beneficial feature of serpentine, which is uniform flow distribution across the electrode, and can enable quick exchange of product and reactant species between the flow channel electrolyte and porous electrode electrolyte.

2. Materials and methods

Characterization of large-scale redox flow battery cells requires thorough hydrodynamic understanding in addition to electrochemical measurements. Flow uniformity and electrolyte substrate through porous electrode cannot be measured experimentally and thus computational predictions play significant role. And, these simulations should be validated with corresponding experimentally measurable quantities like pressure drop and cell voltage. The VRFB cells have been fabricated using graphite bipolar plates (SGL R7650) on which the designed flow field is engraved, graphite felt electrodes (SGL GFD 4.65 EA) and Nafion 117 membrane. The assembled cell has been given an electrode compression ratio of 35 %. Vanadium electrolyte solution (Oxkem) of concentration 1.6 M is used to characterize the cells. Pressure drop has been measured experimentally using air filled inverted U-tube manometer by circulating electrolyte through the assembled cell. The measured pressure drop is used to validate the CFD simulations. Single cell in operation is shown in Fig. 1. A 3-deminsional geometry as shown in Fig. 2a has been developed using ANSYS 2022 R2. The porous nature of graphite felt led to intrusion of its body into cross-section of flow channel as shown in Fig. 2b, c & d. The depth of intrusion of porous electrode is a function of width of flow field channel engraved on graphite bipolar plate and the extent of electrode compression. This feature is considered in the computational design and the corresponding

hydrodynamic simulations have been carried out to predict the velocity and distribution pattern of electrolyte through flow field channels & porous electrode including the associated pressure drop. The required input parameters for the simulations like permeability of electrode, viscosity and density of electrolyte has been measured experimentally. Conventional serpentine flow field is designed with channel dimension (4 × 3 × 3) (channel width × rib width × channel depth). The channel width of 4 mm with 35 % electrode compression has given approximately 1 mm intrusion depth of electrode intrusion [38]. For the measured compression ratios of 18 % and 35 % for under the channel electrode and under the rib electrode of conventional SFF, respectively, the permeabilities are determined as 5.07×10^{-11} m^2 and 3.36×10^{-11} m^2. The density and viscosity of the electrolyte are specified as 1447 kg m^{-3} and 0.004 Pa s, respectively [39].

The boundary conditions for simulations are specified as equal velocity at the inlet pipe, fully developed flow, zero gauge-pressure at the outlet and no-slip boundary condition on the walls of the fluid domain. Flow in the electrodes and channels is obtained by solving the steady, incompressible, Reynolds-averaged Navier-Stokes equations with porous media transport terms included in the porous region. Porous media modelling applied only to the flow on the electrode side. In order to demonstrate sufficient grid resolution (the solution would not significantly change on further refined grid), a grid independency test was conducted. A grid size of 0.25 mm achieved a grid independency from which a further refinement in grid size produced minor variation in results as shown in Fig. 2h. In addition, the grid size of 0.2 mm has produced huge number of grid elements of about 27 million which is twice the number of elements produced by the grid size 0.25 mm. In view of computational resource and time taken to run simulations, the grid size of 0.25 mm was taken as the optimal one and was used to simulate CFD predictions for all other configurations.

Mass conservation

$$\nabla.(\rho \boldsymbol{u}) = 0$$

Momentum conservation for non-porous flow

$$\nabla.(\rho \boldsymbol{u}\boldsymbol{u}) = \nabla.\left(-p\delta\mu\left(\nabla \boldsymbol{u} + (\nabla \boldsymbol{u})^T\right)\right)$$

Momentum conservation for porous flow

$$\nabla.(\rho \boldsymbol{u}\boldsymbol{u}) = \nabla.\left(-p\delta + \mu\left(\nabla \boldsymbol{u} + (\nabla \boldsymbol{u})^T\right)\right) + \left(\frac{-\mu}{K}\right)\boldsymbol{u}$$

here, p is static pressure, u is the velocity vector, ρ is density, μ is viscosity of the fluid, δ is Kronecker delta function and K is the permeability of the porous medium.

In view of the identified feature of serpentine flow field which is fractional split of flow between flow field channels and porous electrode, it is noted that the fraction of electrolyte that is entered into porous electrode; continue to transport convectively through the electrode as a substrate with minimal diffusional exchange with the electrolyte flowing through the flow channels [38]. As the split of electrolyte from flow field to electrode occurs in the very first channel and have possibility of recombining hydrodynamically only in the last flow channel, the residence time for electrolyte species in the electrode increases with increase in cell size. Thus, the product species in the electrolyte of electrode may accumulate leaving the major portion of electrode, which is away from the inlet section starving for reactants. Therefore, there should be a provision to increase exchange of electrolyte species between flow field channels and porous electrode. This study proposes two such provisions. One by having alternate wide and narrow flow field channels as shown in Fig. 2f and another by creating partial slice in the porous electrode as shown in Fig. 2g. The channel width is changed from a constant value of 4 mm to a combination of 5 mm and 3 mm to get wider and narrow combination. In view of change in channel width, the intrusion depth of electrode has been measured to be 1.5 mm and 0.8 mm approximately for the channel widths 5 mm and 3 mm as shown in Fig. 2c and d, respectively at electrode compression ratio of 35 %. Other dimensions like channel depth and rib width kept constant. Although reducing channel depth increase the local momentum, it leads to decrease in the open volume of channel flow in view of intrusion of electrode and can result in huge pressure loss [38]. On the other side, increasing channel depth is detrimental in two aspects as this lead towards increase in thickness of bipolar plate and decrease in local momentum, of which both are not recommended. The other design retains the conventional serpentine configuration on bipolar plate followed by the creation of partial manual slicing in the porous electrode at identified distances along the width of electrode. The number of locations of slicing increases with cell size. In the present study, the traverse distance of electrolyte through electrode is segmented to 1/4th by creating a slicing after every eight flow channels. Through this, a cell area of 625 cm^2 with electrode cross section of 25 cm × 25 cm, creating a slicing after every 8 flow channels resulted three number of slicing which created four segmentations as show in Fig. 2g. All the input parameters used for performing CFD simulations using conventional SFF has been used for the proposed configurations except the permeability of intruded electrode. the permeabilities are determined as 6.32×10^{-11} and 2.82×10^{-11} for the 5 mm and 3 mm channel intrusions, respectively.

The electrolyte which is penetrated into the porous electrode is forced to transport back to the flow field channels due to the developed convective pressure gradient between the adjacent flow channels by the proposed alternate wide and narrow channel combination in the flow field. Thus, it enhances the exchange of electrolyte between flow field channels and porous electrode. In view of added convective transport of electrolyte along with the existing concentration driven diffusive transport between the electrode and flow field, it is assumed to increase the probability of evacuating the reaction products from the electrode and simultaneously replenish the active cites with reactants both by diffusive and convective transport. The provision of slicing in the porous electrode; breaks the path of continuous substrate flow of electrolyte in the electrode and allow merging of it hydrodynamically with electrolyte of the corresponding flow field channel and therefore the subsequent portion of electrode can receive electrolyte consisting of more reactant species compared to the earlier portion of electrode. The flow distribution in these two designs is explored through CFD simulations and compared with that of conventional serpentine. Complimentary experimental studies have also been performed and discussed in detail.

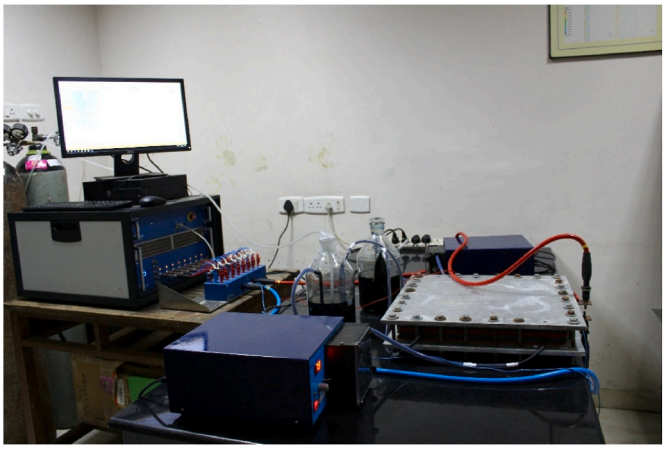

Fig. 1. Single cell in operation with two peristaltic pumps used to circulate the electrolyte from two separate reservoirs to positive and negative side and measuring the electrochemical performance through a battery cycler system.

3. Results and discussion

3.1. Validation of CFD simulations

In order to validate the simulations, redox flow battery cell of active

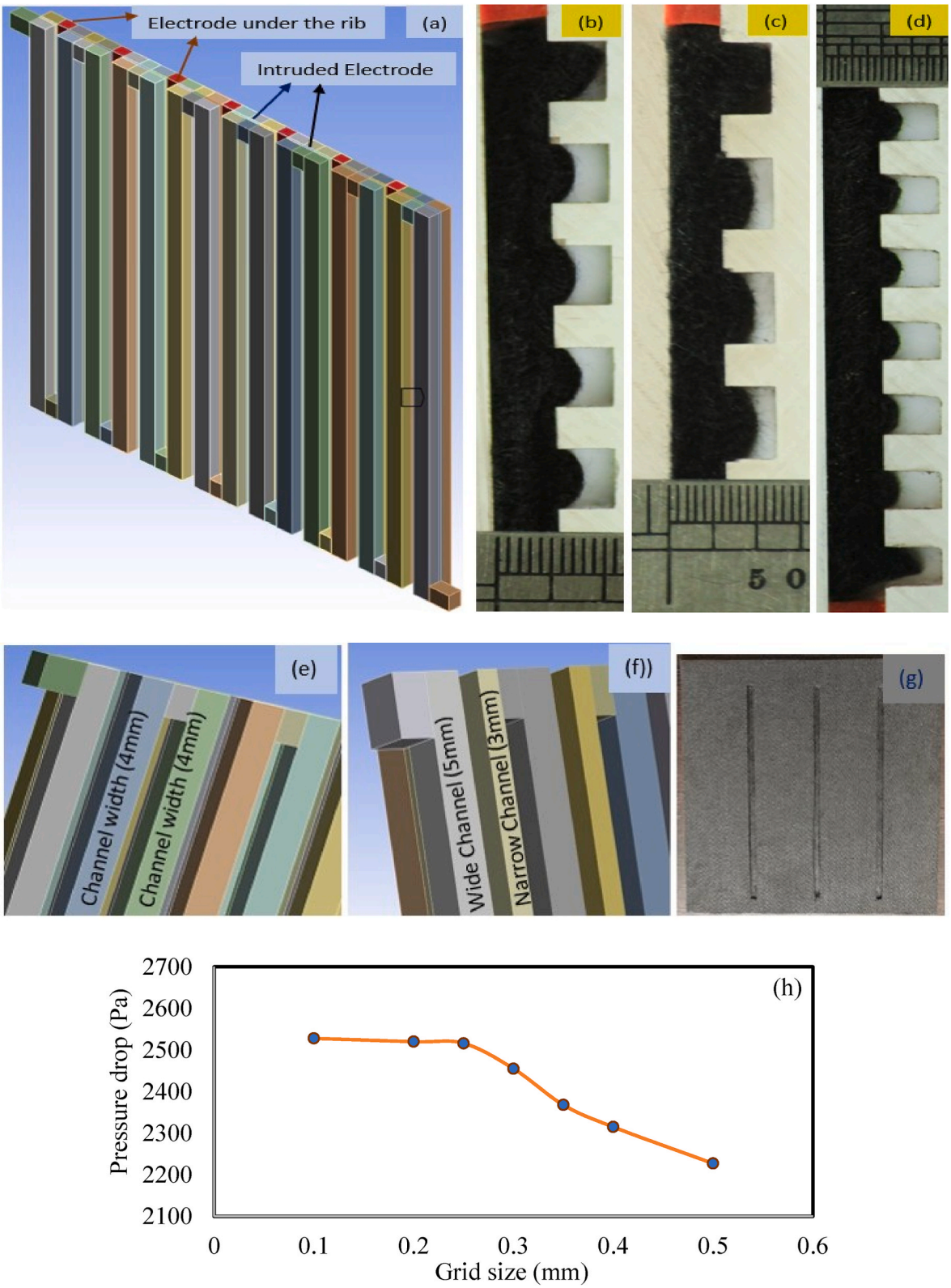

Fig. 2. (a) 3-Dimensional model of flow field and electrode combination, Intrusion of porous electrode into cross-section of flow field channel (b) for channel width of 4 mm, (c) for channel width of 5 mm, & (d) for channel width of 3 mm, (e) Conventional SFF with constant channel dimension (f) alternate wide and narrow flow channels in serpentine flow field, (g) partial slicing of electrode at identified locations and (e) grid independency for CFD simulations.

electrode area of 100 cm^2 (10 cm × 10 cm), with engraved conventional serpentine flow field on bipolar plate, has been assembled and vanadium electrolyte is circulated through the cell at area specific flow rates in the window of 0.2–1.4 $ml.min^{-1}cm^{-2}$ and pressure drop is measured in terms of head difference in the inverted U-tube manometer. In view of the importance of cell size in electrolyte distribution, measurements have been carried out for a cell size of 625 cm^2 (25 cm × 25 cm). CFD simulations are performed at the mentioned flow rates to predict

corresponding pressure drop and the results are compared in Fig. 3a and b with error bars. The maximum deviation between the prediction and measurement is 14 % at both the cell sizes. Similar simulations have been carried out across various cell sizes like 100, 225, 400, 625, 900, 1225, 1600 and 2025 cm^2 for a flow rate of 1.0 $ml.min^{-1}cm^{-2}$ and the predictions are reported in Fig. 3c, d & e. Pressure drop increased with cell size as shown in Fig. 3c and this leads to increase in parasitic losses and reduce the net energy efficiency of a charge-discharge life cycle. In view of this, large size cells may not be recommended with conventional SFF. Velocity of electrolyte in the porous electrode is calculated at the mid depth of electrode and it is averaged by taking at middle, bottom and top sections of electrode. As the inlet flow rate is area specific, average velocity in the porous electrode should remain constant across the cell sizes. However, as can be seen from Fig. 3d, it is changing and increasing with cell size. In view of increased momentum in the flow field channels attributed to their constant cross-section across the cell

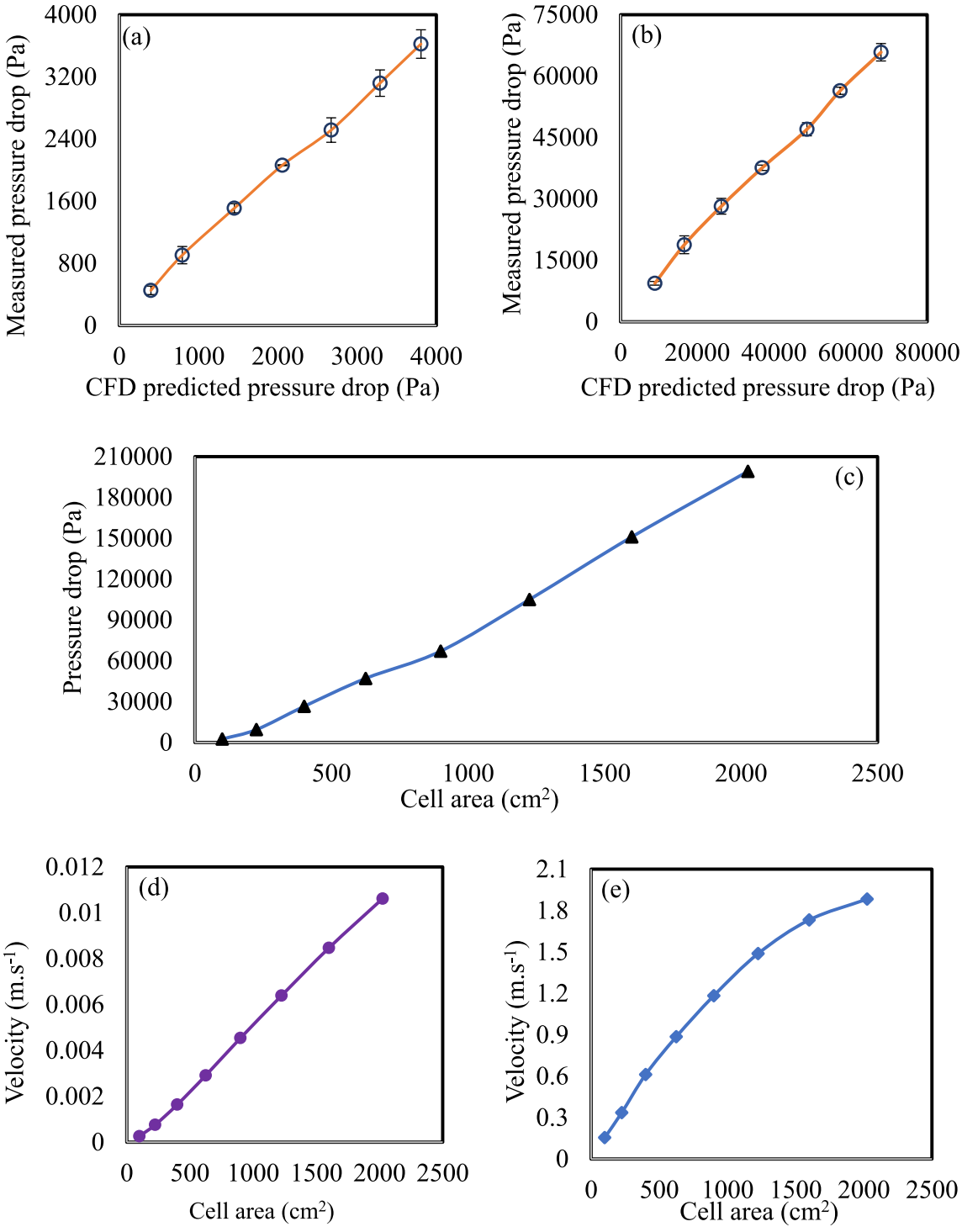

Fig. 3. Comparison of experimentally measured and CFD predicted pressure drop with error bars at various flow rates in the window of 0.2–1.4 $ml.min^{-1}cm^{-2}$ over the cell size (a) 100 cm^2 and (b) 625 cm^2, CFD predicted parameters for a flow rate of 1.0 $ml.min^{-1}cm^{-2}$ across different cell areas (c) pressure drop, (d) electrolyte velocity through porous electrode, and (e) electrolyte velocity through flow field channels.

areas, the fractional split of electrolyte from flow field channels to electrode increases with cell size and it reflects as increased velocity in the electrode with cell size. The constant cross-section of flow field channels across the cell size and increased requirement of volumetric flow rate with cell size, velocity through flow channels should increase and the same is depicted in Fig. 3e. As the fractional split to porous electrode increases with cell size, the increase in flow channel velocity became moderate and therefore resulted in lower increments of velocity through flow channel in cell size towards the larger areas compared to corresponding change in smaller area window. In view of high relative velocity through the flow channels compared to electrode region, pressure loss is majorly governed by the flow through flow channels.

3.2. Electrolyte distribution with conventional serpentine

The fluid flow distribution feature of serpentine flow field can be visualized through Fig. 4. As shown in Fig. 4a, it can be observed that the flow is splitting between the flow field channels and porous electrode with high relative velocity through flow field. The flow of electrolyte through electrode can be best visualized through 3-D fish vectors as shown in Fig. 4b. Electrolyte species that flows through the electrode only will participate in the electrochemical reaction during charge-discharge process, while the same flowing through flow field channels remains unreacted. In order to displace the product species in the electrode, the substrate flow should be discontinued in the electrode and the electrolyte species should travel back to the flow channel. Simultaneously, the same section of electrode should be replenished with the unreacted electrolyte species flowing through flow channels. In view of this, higher number of fishes should be exchanged between flow field channel and electrode and lesser number should flow as a substrate through the electrode to achieve better electrochemical performance. Fig. 4 b, depicts that a smaller number of fishes are exchanging between electrode and flow channel while many are continued to swim through electrode as substrate. This could impact extraction of intrinsic energy of electrolyte and efficiency of charge-discharge life cycles. The fractional distribution of electrolyte through electrode and flow channels can be obtained by determining the velocity quantity throughout the area. The quantum of velocity though electrode region is determined by creating a plane across the depth which traverse through the width of electrode (in the direction of inlet to outlet). Similar planes have been created at the top, middle and bottom portion of electrode (along the length direction) and average of all three is reported as the predicted value. The pattern of electrolyte velocity through the electrode can be captured through this plane and the same is reported in Fig. 5a and b for the cells of active electrode area 100 cm^2 and 625 cm^2, respectively. Similar analysis has also been carried out for flow field channels and the patterns are shown in Fig. 5c and d. The velocity profile shown in Fig. 5a and b depicts uniform availability of electrolyte across the width of electrode. The sine wave in the profile reflects the extent of velocity in the electrode with maximum peak for under the rib and minimum for under the channel electrode portions. In the flow path of electrolyte through porous electrode; velocity is not becoming to near zero while it is moving from under the rib zone to under the channel zone. It conveys that the electrolyte in the electrode is moving continuously as a substrate (as shown in Fig. 4b) having minimal exchange of species with the electrolyte flowing through the flow field channels. And this exchange is being driven by diffusion mass transfer attributed to concentration gradient in the electrolyte. Similar understanding can be obtained from Fig. 5c and d that the velocity across the flow field channels is constant except in the first and last channel. The feed electrolyte splits from flow field channel to electrode in the first channel itself and have the possibility to recombine only in the last flow channel. This phenomenon can be observed more clearly on 625 cm^2 cell shown in Fig. 5d compared to Fig. 5c attributed to the increased fractional split to the electrode with cell size. Once the flow enters into porous zone, it travels as a substrate in the electrode, with minimal and approximately constant exchange with that of flow channel fluid. This led to the constant electrolyte velocity across the flow field channels. Maximum peak of the sine wave in Fig. 5c and d represents velocity near the mid depth of flow field channel and the minimum represent velocity near the wall of the flow field channel towards the rib.

In order to experience the electrolyte distribution pattern with conventional serpentine flow field on scale-up in cell size, velocity profiles through the electrode have been captured and plotted in Fig. 6. The feature of uniform electrolyte distribution across the cross-section of electrode is retained, as shown in Fig. 6, by the conventional SFF across the cell sizes from lab-scale to industrial scale in the window of 100 cm^2–2025 cm^2. Beyond this size, local current distribution, requirement of sophisticated power electronics to deal high current vs. low voltage, material adaptability, leakage due to non-uniform torque and other issues will arise and lead to difficulty in the system management. The pattern of distribution shows flow uniformity and supply of electrolyte species across the entire cross section of electrode in the stack-scale cell sizes with conventional SFF as flow field. In view of the retained flow uniformity and ease of fabrication of such simple serpentine compared to several split designs and complex flow fields, SFF is highly recommendable if pressure drop and electrochemical performance are in the desired window. In view of the substrate flow of electrolyte through electrode, residence time of electrolyte species increases with cell size and need provision to evacuation of products from active sites and simultaneous replenishment with reactant species flowing through flow field channels. Therefore, marginal design modifications are introduced without altering the direction and continuous path way of electrolyte of conventional serpentine with objectives to reduce residence time of products in the electrode and to improve exchange of electrolyte between the electrode and flow field channels. Provision of alternate wide and narrow channels and provision of partial slice in the porous electrode are the proposed marginal designs.

3.3. Electrolyte distribution with proposed marginal design changes

The proposed designs have been introduced into the conventional serpentine and the simulations are carried out to explore the impact on hydrodynamics across the electrode and flow field channels. The predictions are described in Fig. 7. The wide and narrow channel combination enable immediate increase in exchange of porous electrolyte with that of flow field electrolyte as shown in Fig. 7a. The differential momentum created between the flow channels attributing to change in velocity is forcing the exchange of electrolyte between the porous electrode and flow field channels. As can be seen from Fig. 4c, high number of fishes are moving to flow channel from the electrode under wider channel compared to the electrode under narrow channel, with low and high substrate flow through the respective electrode sections. As the evacuation of electrolyte species from the active sites of porous electrode increased, this could lead to low residence time of reaction products and the simultaneous replenishment of electrode sites with reactants from flow field electrolyte; together should give us improved reaction kinetics and increase in energy transaction in a charge-discharge life cycle. The impact of second approach which is creating a partial slice in the porous electrode by retaining the conventional serpentine on bipolar plate is described in Fig. 7b. The fractional electrolyte splitting into porous electrode demonstrates its substrate flow characteristic until it finds break in the form of slice cavity in porous electrode. At this location, majority of the electrolyte species of electrode merge with electrolyte species flowing through flow channels as can be seen from Fig. 4d. Till this; as the electrolyte spends considerable residence time in the electrode, the substrate must have added product species in the path line. This creates huge concentration gradient between the electrode and flow field channels and enable diffusional exchange of species. With this forced convective transport of electrolyte between the flow channel and electrode attributed to the creation of segmentation in the substrate flow path line and diffusional exchange of

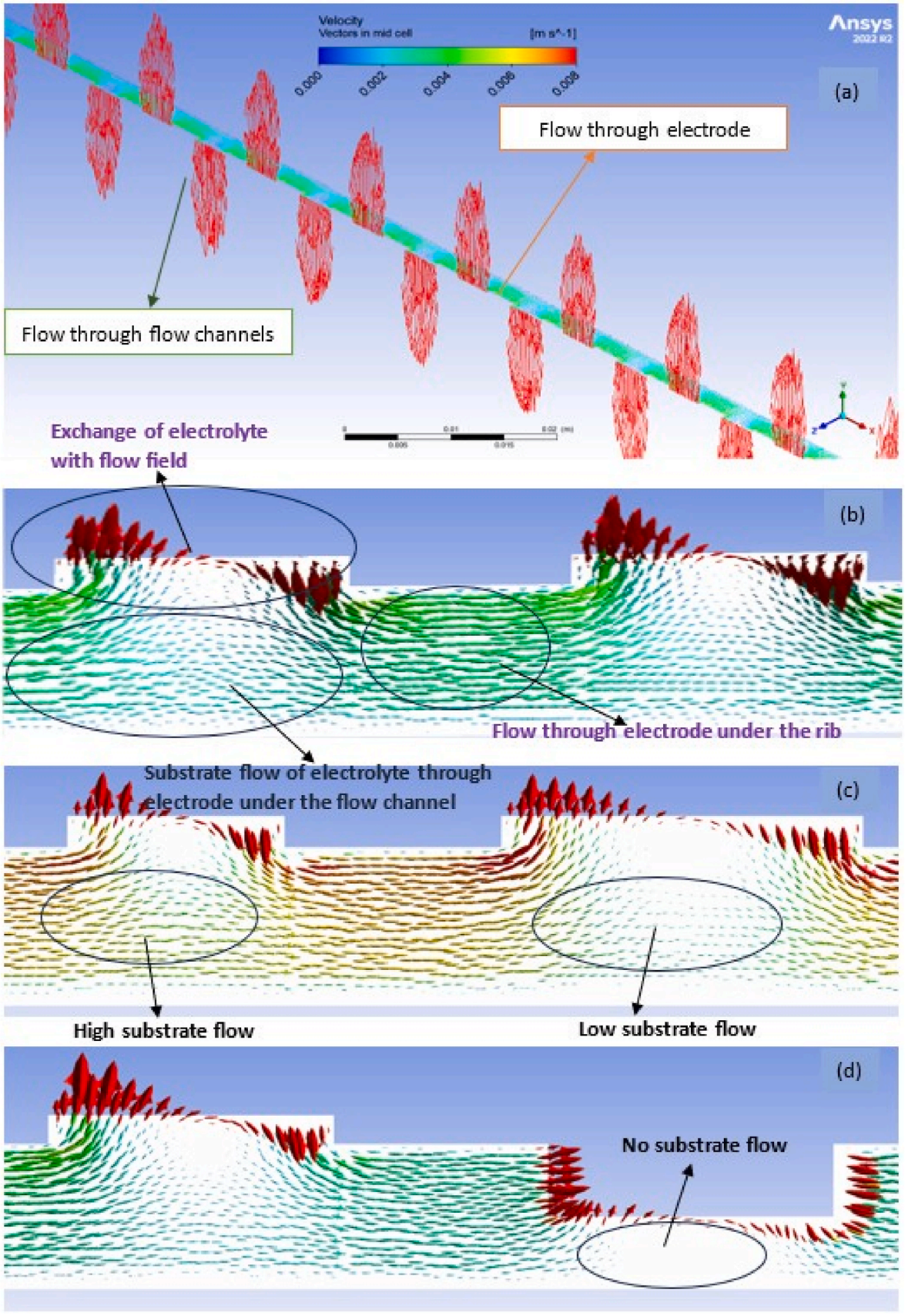

Fig. 4. (a) Velocity vectors showing split flow of electrolyte between flow field channels and electrode. Description of flow through electrode with (b) conventional serpentine flow field, (c) wide and narrow channel combination and (d) Electrode having partial slice.

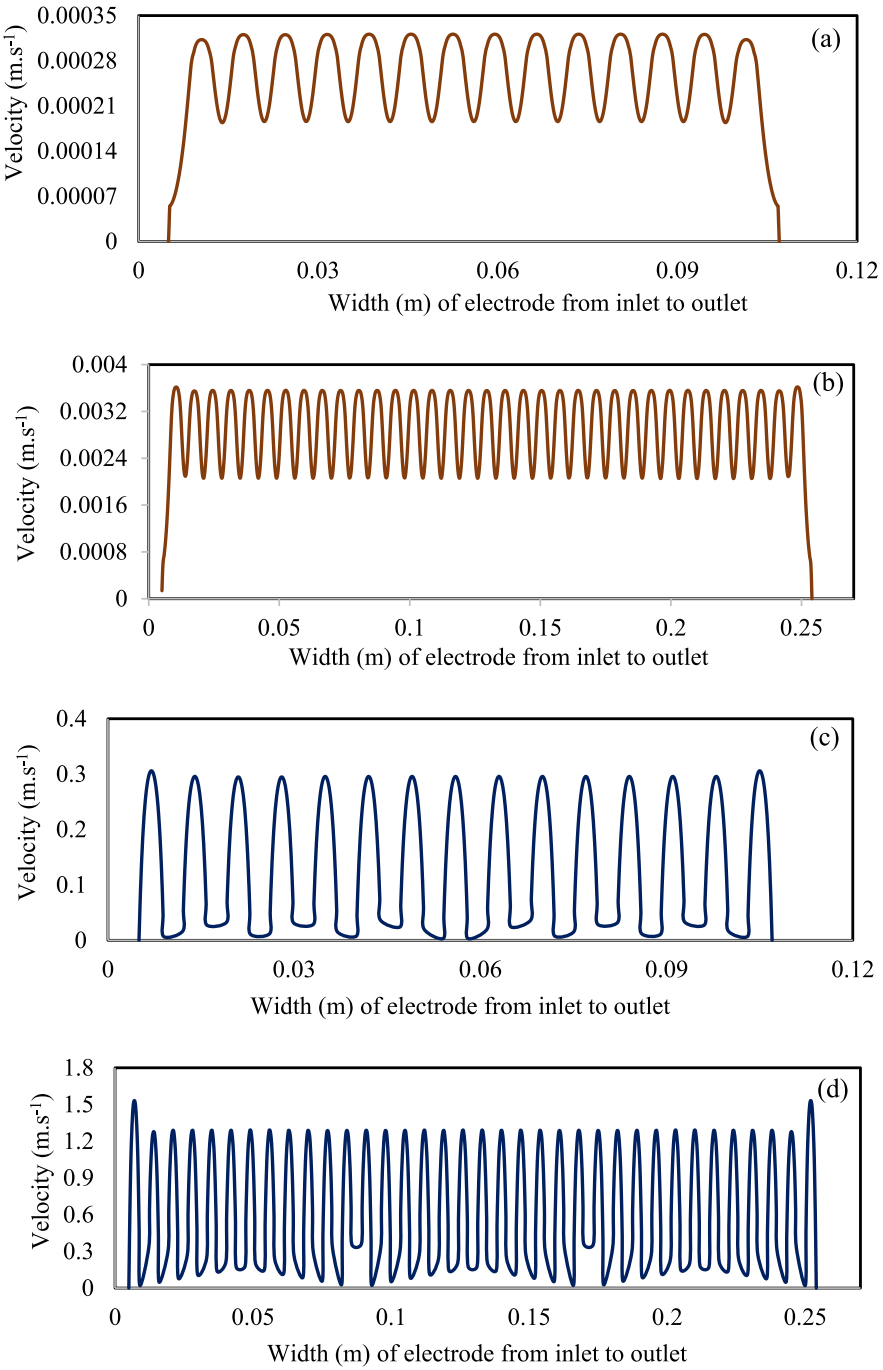

Fig. 5. Electrolyte distribution for a flow rate of 1.0 ml min^{-1}. cm^{-2} in a flow battery cell equipped with conventional serpentine, in the (a) porous electrode of cell area 100 cm^2 (10 cm × 10 cm), (b) porous electrode of cell area 625 cm^2 (25 cm × 25 cm); and (c) flow field channels of cell area 100 cm^2, (d) flow field channels of cell area 625 cm^2.

species together at the slice location; the subsequent electrode portion might receive an electrolyte stream consisting more reactants compared to immediate electrode preceding the slice cavity. The cell of active electrode area 625 cm^2 involves three such slice creations in the electrode and this reduces residence time of substrate species compared to the electrode without slice creations. The impact of these designs on electrochemical characteristics is measured experimentally on this cell size and corresponding improvement in energy density and energy efficiency of a life cycle is discussed.

3.4. Electrochemical characterization

A cell of active area 100 cm^2 has been assembled with conventional serpentine flow field subjected to electrode compression ratio of 35 % and 100 ml of electrolyte volume is taken on each side of reservoirs. Peristaltic pumps are used to circulate electrolyte through the cells. Battery cycler of the capacity 9 V-120 A (Biologic) is used to charge and discharge the cells. The charge-discharge life cycles have been conducted for a current density of 90 mA. cm^{-2} at a flow rate of 1.0 ml min^{-1}. cm^{-2}. These tests will give energy transaction during charge and discharge with corresponding energy efficiency of the cycle. Voltage cut-

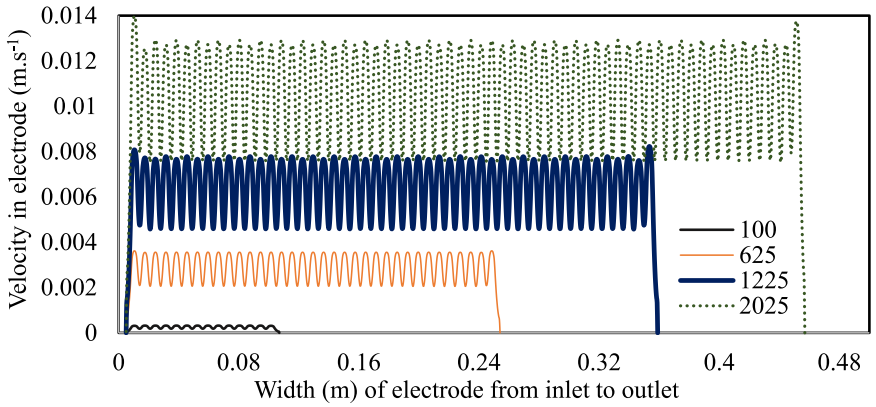

Fig. 6. Electrolyte distribution for a flow rate of 1.0 ml min^{-1}. cm^{-2} in flow battery cells of various sizes from 100 cm^2 to 2025 cm^2 all equipped with conventional serpentine flow field.

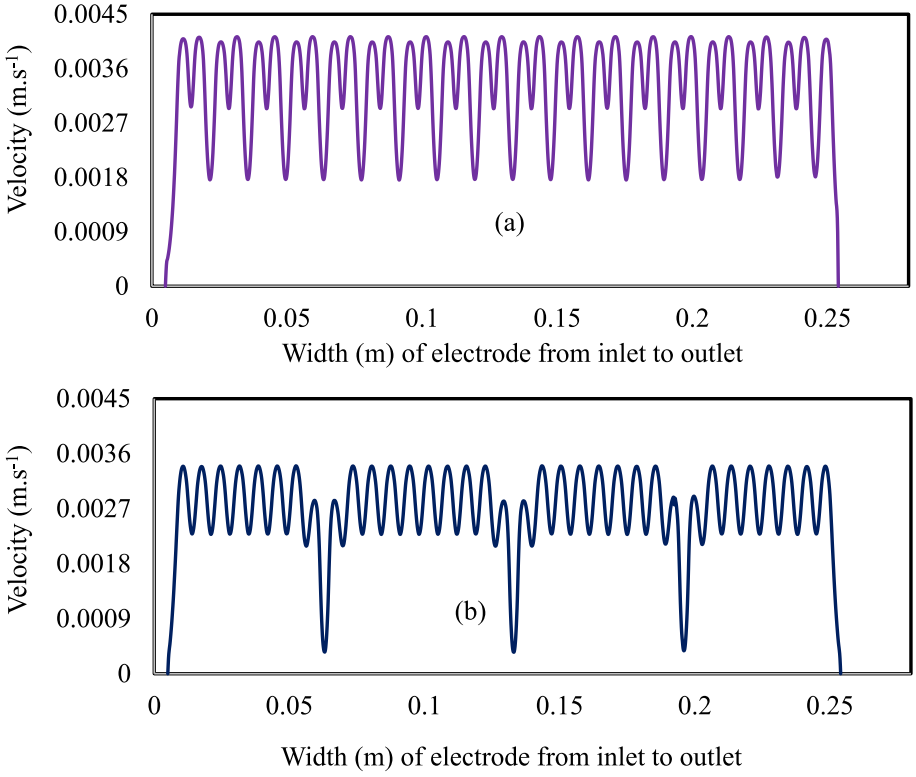

Fig. 7. Electrolyte distribution for a flow rate of 1.0 ml min^{-1}. cm^{-2} in flow battery cell of active area 625 cm^2 engraved with simple conventional serpentine flow field incorporated with (a) wide and narrow channel combination and (b) partial slices in the porous electrode.

off limits are defined as 1.8 V for charging and 0.8 V for discharging. In view instability of V^{2+} in presence of oxygen, nitrogen gas is bubbled through the negative electrolyte to avoid oxidation of electrolyte species during these tests. Three other VRFB cells of active area 625 cm^2 are assembled each having same materials of membrane, electrode, electrolyte and designed at equal electrode compression ratio of 35 %. Only the difference between these three cells is the type of flow field configuration. The first cell is engraved with conventional serpentine, second one with conventional serpentine incorporating alternate wide and narrow channel combination and the third one retain conventional serpentine as of first cell but the electrode is subjected to partial slices as mentioned in Fig. 2g. All the three cells have been subjected to equal operating conditions and the electrochemical measurements are performed. Electrolyte volume of 625 ml is taken on each side of reservoirs. Results of these experiments are plotted in Fig. 8.

Every cell has been demonstrated with 40 charge-discharge life cycles for a flow rate of 1.0 ml min^{-1}. cm^{-2} at current density of 90 mA. cm^{-2}, and Fig. 8a & b are plotted with 3rd cycle. As can be depicted from Fig. 8a, the discharged capacity per litre of electrolyte has been decreased from 25 Ah. L^{-1} to 22.4 Ah. L^{-1} as the cell size increased from 100 to 625 cm^2 keeping all the design and operating conditions same. This can be attributed to increased fractional split of electrolyte from flow field channels to the electrode leading to more substrate flow and high residence time of product species in the electrode, with cell size. Similar results have been reported in our earlier studies [36]. As can be seen from Fig. 8b, difference in the cell voltage across the cells is becoming higher towards the end of life-cycle. During initial stage of charge and discharge process, the state of charge of electrolyte is high with the corresponding reactants (VO^{2+} and V^{3+} during charge and VO_2^+ and V^{2+} during discharge at positive side and negative side,

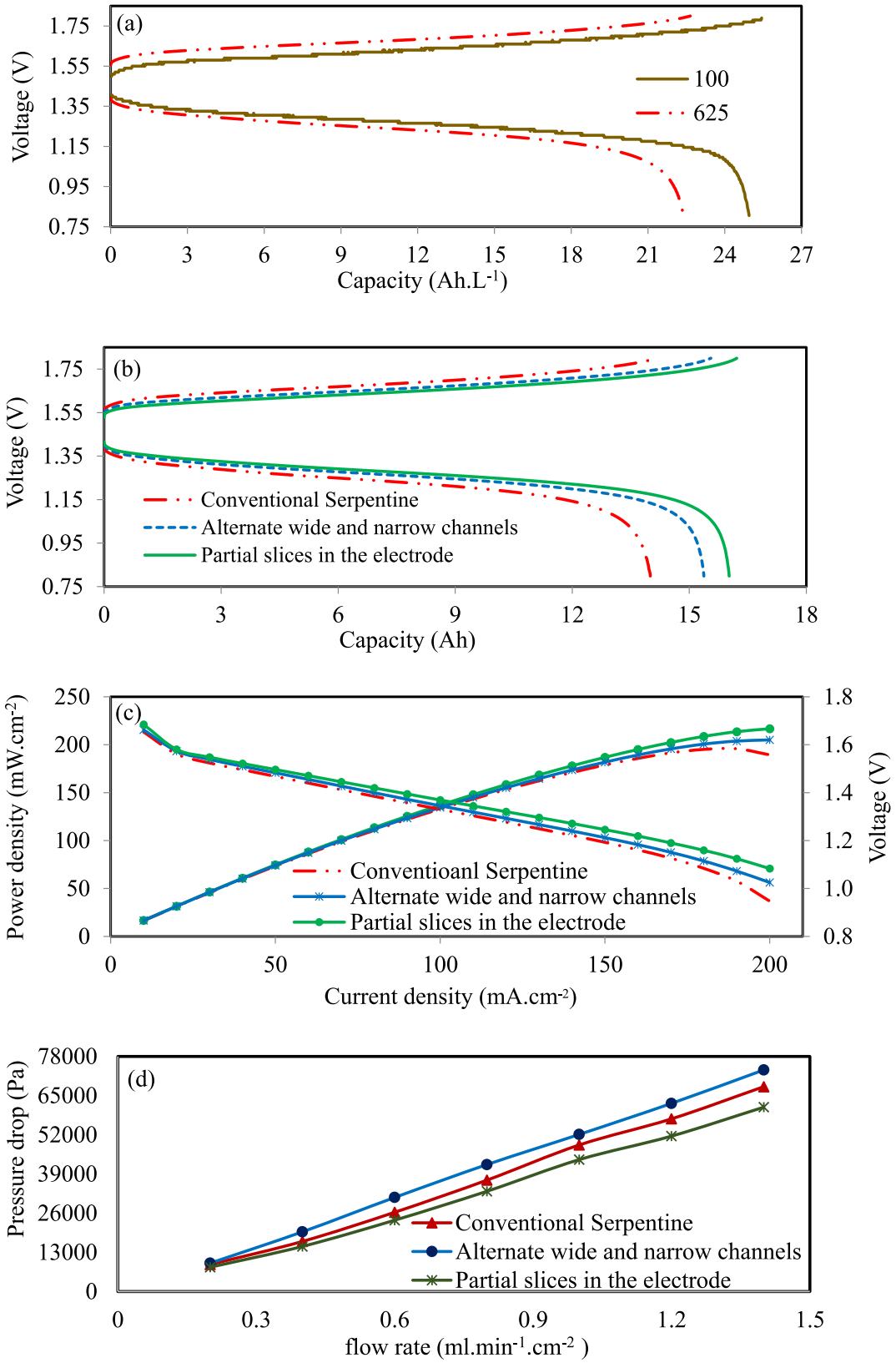

Fig. 8. Electrochemical measurements at flow rate of 1.0 ml min^{-1}. cm^{-2} with (a) comparison of life cycle performance at current density of 90 mA. cm^{-2} for the cells of active area 100 cm^2 and 625 cm^2 both equipped with conventional serpentine flow field, and similar studies on cells of active electrode area 625 cm^2 equipped with different flow fields towards (b) charge-discharge life cycles at current density of 90 mA. cm^{-2} and (c) power density at the constant mentioned flow rate with varying current density up to 200 mA. cm^{-2}, (d) measured pressure drop in the cells of 625 cm^2 configure with conventional SFF and proposed designs.

respectively) and eventually these are getting converted to products (VO_2^+ and V^{2+} during charge and VO^{2+} and V^{3+} during discharge at positive side and negative side, respectively) on the active cites of electrode. Due to high substrate flow of electrolyte species in the electrode with low exchange with that of electrolyte flowing through flow channels in the conventional serpentine, it is subjected to early mass transfer polarization compared to other cells. In view of increased probability of exchange of species between electrode and flow field, the second and third cells have been delayed in mas transfer polarization and able to extract increased amount of intrinsic energy with the same amount of electrolyte compared to first cell. The quantitative metrics in the form of capacity are 14 Ah, 15.37 Ah and 16 Ah, respectively for the first, second and third cells. The same when converted to energy (by integrating capacity with cell voltage), these have given 19.4 Wh, 21.7 Wh and 22.7 Wh which becomes as 31.1 Wh. L^{-1}, 34.7 Wh. $L^{-1}$and 36.4 Wh. L^{-1} when represent in the form of energy density, respectively for the cells. The cell designed with partial slice in the electrode (third cell) without altering the conventional serpentine flow field on bipolar plate has been given an increment of 17 % in energy density. Energy efficiency has also been measured through coulombic and voltage efficiencies, and these obtained as 71.8 %, 73.6 % and 74.8 % respectively for the cells at the operated current density of 90 mA. cm^{-2}. On the parasitic loss front, the proposed designs have not seen significant benefits. The measured pressure drops in these three cells at the chosen flow rate of 1.0 ml min^{-1} cm^{-2} are 48.6 kPa, 52.1 kPa and 46.7 kPa, respectively. The slight increase in pressure loss in the cell with wide and narrow channel combination is attributed to local head losses between the adjacent channels. The inclusion of pumping losses in finding net energy efficiency of life cycles gave 71.2 %, 72.8 and 74.3 %, respectively. During the demonstrated 40 life cycles, the observed capacity fade is approximately similar in these three cells and it is about 0.4 % per cycle. Although the fade in capacity is a function of crossover of electrolyte species through membrane, parasitic side reactions and material degradation; the effect of creating cavity on electrode on the capacity fade need to be investigated through prolonged life cycles. In addition to life cycles tests, polarization studies are conducted on these three cells to determine maximum power density, and the results are presented in Fig. 8c. In view of current rating limitation in the battery cycler, the measurement is limited up to a current density of 200 mA. cm^{-2}. The cell with partial slice in the electrode could able to obtain a power density of 217 mW. cm^{-2} at a current density of 200 mA. cm^{-2} and still has the provision to operate for higher currents as the cell voltage has reached only to 1.08 V having its cut-off voltage at 0.8 V. Whereas the first cell with conventional serpentine has seen 190 mW. cm^{-2} as peak power density at a current density of 190 mA. cm^{-2} and commenced downfall at current density of 200 mA. cm^{-2}.

The early onset of mass transfer (concentration) polarization with simple conventional serpentine in view of its substrate flow with minimal exchange of species between electrode and flow field posing limitations to adapt it for large-scale cell sizes. The proposed marginal design changes assisted in improving the exchange of species between electrode and flow field channels. The proposed design of having partial slice in the electrode without altering the conventional serpentine flow field on bipolar plate is highly recommendable for application in large-scale vanadium redox flow batteries. However, further studies are recommended to streamline the location of segmentation of substrate flow in the electrode, the effect of loss of number of active sites on the effect of electrochemical reaction. An electrochemical model incorporating the hydrodynamics could provide the speed of reaction and concentration profile of species between the electrode and flow field channels, and supported electrochemical investigation is needed especially at larger cells for fine-tuning the proposed design.

4. Conclusions

Serpentine flow field is proved to be superior in extracting better electrochemical performance compared to other flow fields when used in lab-scale vanadium redox flow batteries. Nevertheless, these have not been explored at large size cells which is imperative for the industrial stacks. This study involves thorough understanding on the features of serpentine flow field, subsequent impact with scale-up in cell size and suitable modifications needed to adapt it for application in large-scale vanadium redox flow batteries. Following conclusions can be drawn from the present study.

- Investigation on conventional serpentine flow field demonstrated that the uniform distribution feature has been retained during the scale-up of cell size from lab-scale to stack-scale, however with increase in substrate flow of electrolyte through electrode and parasitic pumping losses.
- The proposed alternate wide and narrow channel combination in the geometry of serpentine flow field enabled increased exchange of electrolyte between the electrode and flow field, yet with marginal increase in pressure loss
- The proposed creation of partial slice in the electrode without altering the conventional serpentine flow field enabled merging of electrolyte substrate of electrode with flow field electrolyte and can supply electrolyte stream of higher reactant concentration to the subsequent portion of electrode compared to immediately preceding electrode
- Electrochemical experiments revealed advantage of the proposed designs by extracting more amount of intrinsic energy per litre of electrolyte at higher energy efficiency. Creation of partial slice in the electrode at identified locations gave 17 % enhancement in the energy density and 3 % increment in the energy efficiency of a life cycle
- Thus, creation of cavity through partial slicing in the porous electrode combined with conventional simple serpentine flow field is highly economical and suitable for application in large-scale vanadium redox flow batteries.

CRediT authorship contribution statement

Raveendra Gundlapalli: Writing – original draft, Visualization, Supervision, Resources, Project administration, Methodology, Investigation, Funding acquisition, Conceptualization. **Gaurav Jaiswal:** Writing – review & editing, Validation, Software, Data curation.

Declaration of competing interest

The authors declare that they have no known competing financial interests or personal relationships that could have appeared to influence the work reported in this paper.

Acknowledgements

This work was supported by the Seed grant (Grant No: 19-(05)/2024-25/10625) by Indian Institute of Technology (BHU) Varanasi and it is gratefully acknowledged.

Data availability

Data will be made available on request.

References

[1] E. Sánchez-Díez, E. Ventosa, M. Guarnieri, A. Trovò, C. Flox, R. Marcilla, F. Soavi, P. Mazur, E. Aranzabe, R. Ferret, Redox flow batteries: status and perspective towards sustainable stationary energy storage, J. Power Sources 481 (2021), https://doi.org/10.1016/j.jpowsour.2020.228804.

[2] A.A. Kurilovich, A. Trovò, M. Pugach, K.J. Stevenson, M. Guarnieri, Prospect of modeling industrial scale flow batteries – from experimental data to accurate overpotential identification, Renew. Sustain. Energy Rev. 167 (2022), https://doi.org/10.1016/j.rser.2022.112559.

[3] M.M. Rahman, M.M. Islam, M. Shafiullah, MdA. Islam, M.A.R. Chowdhury, MdH. Zahir, Advancing grid integration with redox flow batteries: an engineering and economic review, Green Chem. Lett. Rev. 18 (2025), https://doi.org/10.1080/17518253.2025.2507333.
[4] M. Skyllas-Kazacos, Review—highlights of UNSW all-vanadium redox battery development: 1983 to present, J. Electrochem. Soc. (2022), https://doi.org/10.1149/1945-7111/ac7bab.
[5] J. Du, J. Liu, S. Liu, L. Wang, K.C. Chou, Research progress of vanadium battery with mixed acid system: a review, J. Energy Storage 70 (2023) 107961, https://doi.org/10.1016/J.EST.2023.107961.
[6] P. Alotto, M. Guarnieri, F. Moro, Redox flow batteries for the storage of renewable energy: a review, Renew. Sustain. Energy Rev. 29 (2014) 325–335, https://doi.org/10.1016/j.rser.2013.08.001.
[7] R. Gundlapalli, S. Kumar, S. Jayanti, Stack design considerations for vanadium Redox flow battery, INAE Lett. (2018), https://doi.org/10.1007/s41403-018-0044-1.
[8] Z. Rhodes, J.R. Cabrera-Pardo, M. Li, S.D. Minteer, Electrochemical advances in non-aqueous redox flow batteries, Isr. J. Chem. 61 (2021) 101–112, https://doi.org/10.1002/IJCH.202000049.
[9] A. Tang, J. Bao, M. Skyllas-Kazacos, Dynamic modelling of the effects of ion diffusion and side reactions on the capacity loss for vanadium redox flow battery, J. Power Sources 196 (2011) 10737–10747, https://doi.org/10.1016/j.jpowsour.2011.09.003.
[10] A. Tang, J. Bao, M. Skyllas-Kazacos, Studies on pressure losses and flow rate optimization in vanadium redox flow battery, J. Power Sources 248 (2014) 154–162, https://doi.org/10.1016/j.jpowsour.2013.09.071.
[11] Z. Huang, A. Mu, L. Wu, B. Yang, Y. Qian, J. Wang, Comprehensive analysis of critical issues in all-vanadium Redox flow battery, ACS Sustain. Chem. Eng. 10 (2022) 7786–7810, https://doi.org/10.1021/acssuschemeng.2c01372.
[12] R. Gundlapalli, S. Jayanti, Comparative study of kilowatt-scale vanadium redox flow battery stacks designed with serpentine flow fields and split manifolds, Batteries 7 (2021), https://doi.org/10.3390/batteries7020030.
[13] N. Gurieff, C.Y. Cheung, V. Timchenko, C. Menictas, Performance enhancing stack geometry concepts for redox flow battery systems with flow through electrodes, J. Energy Storage 22 (2019) 219–227, https://doi.org/10.1016/j.est.2019.02.014.
[14] X. Ke, J.M. Prahl, J.I.D. Alexander, J.S. Wainright, T.A. Zawodzinski, R.F. Savinell, Rechargeable redox flow batteries: flow fields, stacks and design considerations. https://doi.org/10.1039/c8cs00072g, 2018.
[15] D.J. Park, K.S. Jeon, C.H. Ryu, G.J. Hwang, Performance of the all-vanadium redox flow battery stack, J. Ind. Eng. Chem. 45 (2017) 387–390, https://doi.org/10.1016/j.jiec.2016.10.007.
[16] B. Sun, M. Skyllas-Kazacos, Chemical modification of graphite electrode materials for vanadium redox flow battery application-part II. Acid treatments, Electrochim. Acta 37 (1992) 2459–2465, https://doi.org/10.1016/0013-4686(92)87084-D.
[17] P.C. Ghimire, A. Bhattarai, R. Schweiss, G.G. Scherer, N. Wai, A comprehensive study of electrode compression effects in all vanadium redox fl ow batteries including locally resolved measurements, Appl. Energy 230 (2018) 974–982, https://doi.org/10.1016/j.apenergy.2018.09.049.
[18] S. Roe, C. Menictas, M. Skyllas-Kazacos, A high energy density vanadium Redox flow battery with 3 M vanadium electrolyte, J. Electrochem. Soc. 163 (2016) A5023–A5028, https://doi.org/10.1149/2.0041601jes.
[19] C. Zhang, T.S. Zhao, Q. Xu, L. An, G. Zhao, Effects of operating temperature on the performance of vanadium redox flow batteries, Appl. Energy 155 (2015) 349–353, https://doi.org/10.1016/j.apenergy.2015.06.002.
[20] R. Gundlapalli, S. Jayanti, Case studies of operational failures of vanadium redox flow battery stacks, diagnoses and remedial actions, J. Energy Storage i (2020), https://doi.org/10.1016/j.est.2020.102078.
[21] X. Ma, H. Zhang, C. Sun, Y. Zou, T. Zhang, An optimal strategy of electrolyte flow rate for vanadium redox flow battery, J. Power Sources 203 (2012) 153–158, https://doi.org/10.1016/j.jpowsour.2011.11.036.
[22] H. Chen, S. Wang, H. Gao, X. Feng, C. Yan, A. Tang, Analysis and optimization of module layout for multi-stack vanadium flow battery module, J. Power Sources 427 (2019) 154–164, https://doi.org/10.1016/j.jpowsour.2019.04.054.
[23] R. Gundlapalli, A. Bhattarai, R. Ranjan, P.C. Ghimire, X. Min, N. Afiq, B. Zainudin, N. Wai, F. Mahlendorf, A. Jasincuk, H. Thorsten, Characterization and scale-up of serpentine and interdigitated flow fields for application in commercial vanadium redox flow batteries, J. Power Sources 542 (2022) 231812, https://doi.org/10.1016/j.jpowsour.2022.231812.
[24] Q. Xu, T.S. Zhao, C. Zhang, Performance of a vanadium redox flow battery with and without flow fields, Electrochim. Acta 142 (2014) 61–67, https://doi.org/10.1016/j.electacta.2014.07.059.
[25] S. Maurya, P.T. Nguyen, Y.S. Kim, Q. Kang, R. Mukundan, Effect of flow field geometry on operating current density, capacity and performance of vanadium redox flow battery, J. Power Sources 404 (2018) 20–27, https://doi.org/10.1016/j.jpowsour.2018.09.093.
[26] M. Messaggi, P. Canzi, R. Mereu, A. Baricci, F. Inzoli, A. Casalegno, M. Zago, Analysis of flow field design on vanadium redox flow battery performance: development of 3D computational fluid dynamic model and experimental validation, Appl. Energy 228 (2018) 1057–1070, https://doi.org/10.1016/j.apenergy.2018.06.148.
[27] S. Kumar, S. Jayanti, Effect of flow field on the performance of an all-vanadium redox flow battery, J. Power Sources 307 (2016) 782–787, https://doi.org/10.1016/j.jpowsour.2016.01.048.
[28] M. Macdonald, R.M. Darling, Comparing velocities and pressures in redox flow batteries with interdigitated and serpentine channels, AIChE J. 65 (2019) 1–11, https://doi.org/10.1002/aic.16553.
[29] B.W. Zhang, Y. Lei, B.F. Bai, T.S. Zhao, A two-dimensional model for the design of flow fields in vanadium redox flow batteries, Int. J. Heat Mass Tran. 135 (2019) 460–469, https://doi.org/10.1016/j.ijheatmasstransfer.2019.02.008.
[30] Q. He, J. Yu, Z. Guo, J. Sun, S. Zhao, T. Zhao, M. Ni, Modeling of vanadium redox flow battery and electrode optimization with different flow fields, E-Prime - advances in electrical engineering, Electron. Energy 1 (2021), https://doi.org/10.1016/j.prime.2021.100001.
[31] Z. Huang, A. Mu, Flow field design and performance analysis of vanadium redox flow battery, Ionics (2021), https://doi.org/10.1007/s11581-021-04213-8.
[32] Z.N. Duan, G.B. Zhang, J.F. Zhang, Z.G. Qu, Experimental investigation on the performance characteristics of flow fields in redox flow batteries under various electrode parameters, Front. Therm. Eng. 2 (2022) 1–16, https://doi.org/10.3389/fther.2022.931160.
[33] E. Knudsen, P. Albertus, K.T. Cho, A.Z. Weber, A. Kojic, Flow simulation and analysis of high-power flow batteries, J. Power Sources 299 (2015) 617–628, https://doi.org/10.1016/j.jpowsour.2015.08.041.
[34] J. Sun, M. Zheng, Z. Yang, Z. Yu, Flow field design pathways from lab-scale toward large-scale flow batteries, Energy 173 (2019) 637–646, https://doi.org/10.1016/j.energy.2019.02.107.
[35] R. Su, Z. Wang, Y. Cai, J. Ying, H. Li, T. Zhao, H. Jiang, Scaling up flow fields from lab-scale to stack-scale for redox flow batteries, Chem. Eng. J. 486 (2024) 149946, https://doi.org/10.1016/J.CEJ.2024.149946.
[36] R. Gundlapalli, S. Jayanti, E ff ect of electrolyte convection velocity in the electrode on the performance of vanadium redox fl ow battery cells with serpentine fl ow fi elds, J. Energy Storage 30 (2020) 101516, https://doi.org/10.1016/j.est.2020.101516.
[37] R. Gundlapalli, S. Jayanti, Effective splitting of serpentine flow field for applications in large-scale flow batteries, J. Power Sources 487 (2021) 229409, https://doi.org/10.1016/j.jpowsour.2020.229409.
[38] R. Gundlapalli, S. Jayanti, Effect of channel dimensions of serpentine flow fields on the performance of a vanadium redox flow battery, J. Energy Storage 23 (2019) 148–158, https://doi.org/10.1016/j.est.2019.03.014.
[39] R. Gundlapalli, S. Jayanti, Effect of electrode compression and operating parameters on the performance of large vanadium redox flow battery cells, J. Power Sources 427 (2019) 231–242, https://doi.org/10.1016/j.jpowsour.2019.04.059.
[40] L.F. Arenas, J.J.H. Pijpers, Hydraulic Aspects of Redox Flow Batteries: Flow Fields and Hydraulic Circuits, Elsevier Inc., 2021, https://doi.org/10.1016/B978-0-12-819723-3.00073-1.
[41] Z. Wang, R. Su, H. Jiang, T. Zhao, Understanding and enhancing the under-rib convection for flow-field structured vanadium redox flow batteries, Int. J. Heat Mass Tran. 230 (2024) 125789, https://doi.org/10.1016/J.IJHEATMASSTRANSFER.2024.125789.
[42] M.Y. Lu, C. Yin, Q. Ma, H.N. Su, P. Lu, Z.Q. Dai, W.W. Yang, Q. Xu, Flow field structure design for redox flow battery: developments and prospects, J. Energy Storage 95 (2024) 112303, https://doi.org/10.1016/J.EST.2024.112303.
[43] Z. Huang, A. Mu, L. Wu, H. Wang, Vanadium redox flow batteries: flow field design and flow rate optimization, J. Energy Storage 45 (2022), https://doi.org/10.1016/j.est.2021.103526.
[44] J. Sun, M. Zheng, Y. Luo, Z. Yu, Three-dimensional detached serpentine flow field design for redox flow batteries, J. Power Sources 428 (2019) 136–145, https://doi.org/10.1016/j.jpowsour.2019.04.106.
[45] M.Y. Lu, Y.M. Deng, W.W. Yang, M. Ye, Y.H. Jiao, Q. Xu, A novel rotary serpentine flow field with improved electrolyte penetration and species distribution for vanadium redox flow battery, Electrochim. Acta 361 (2020) 137089, https://doi.org/10.1016/j.electacta.2020.137089.
[46] H. Sharma, M. Kumar, Enhancing power density of a vanadium redox flow battery using modified serpentine channels, J. Power Sources 494 (2021) 229753, https://doi.org/10.1016/j.jpowsour.2021.229753.
[47] M.Y. Lu, Y.H. Jiao, X.Y. Tang, W.W. Yang, M. Ye, Q. Xu, Blocked serpentine flow field with enhanced species transport and improved flow distribution for vanadium redox flow battery, J. Energy Storage 35 (2021) 102284, https://doi.org/10.1016/j.est.2021.102284.
[48] M. Messaggi, C. Gambaro, A. Casalegno, M. Zago, Development of innovative flow fields in a vanadium redox flow battery: design of channel obstructions with the aid of 3D computational fluid dynamic model and experimental validation through locally-resolved polarization curves, J. Power Sources 526 (2022) 231155, https://doi.org/10.1016/j.jpowsour.2022.231155.
[49] L. Pan, J. Xie, J. Guo, D. Wei, H. Qi, H. Rao, P. Leung, L. Zeng, T. Zhao, L. Wei, In-plane gradient design of flow fields enables enhanced convections for redox flow batteries, Energy Advances 2 (2023) 2006–2017, https://doi.org/10.1039/D3YA00365E.

[50] B. Akuzum, Y.C. Alparslan, N.C. Robinson, E. Agar, E.C. Kumbur, Obstructed flow field designs for improved performance in vanadium redox flow batteries, J. Appl. Electrochem. 49 (2019) 551–561, https://doi.org/10.1007/s10800-019-01306-1.
[51] Y. Liu, Z. Huang, X. Xie, Y. Liu, J. Wu, Z. Guo, Q. Huang, Redox flow battery:flow field design based on bionic mechanism with different obstructions, Chem. Eng. J. 498 (2024) 155663, https://doi.org/10.1016/J.CEJ.2024.155663.
[52] B. Yang, A. Mu, J. Wang, Y. Wang, W. Wang, Bioinspired flow fields: a numerical investigation into nature-mimicking designs for boosting vanadium redox flow batteries, Chem. Eng. Sci. 298 (2024) 120440, https://doi.org/10.1016/J.CES.2024.120440.
[53] L.D. Brown, T.P. Neville, R. Jervis, T.J. Mason, P.R. Shearing, D.J.L. Brett, The effect of felt compression on the performance and pressure drop of all-vanadium redox flow batteries, J. Energy Storage 8 (2016) 91–98, https://doi.org/10.1016/j.est.2016.10.003.
[54] D. Reed, E. Thomsen, B. Li, W. Wang, Z. Nie, B. Koeppel, J. Kizewski, V. Sprenkle, Stack developments in a kW class all vanadium mixed acid Redox flow battery at the Pacific Northwest national laboratory, J. Electrochem. Soc. 163 (2016) A5211–A5219, https://doi.org/10.1149/2.0281601jes.